JOURNAL OF THERMOPHYSICS AND HEAT TRANSFER
Vol. 18, No. 1, January–March 2004

Axisymmetric Impingement Heat Transfer with a Nonlinear k–ε Model

B. Merci,* C. De Langhe,† K. Lodefier,† and E. Dick‡
Ghent University, B-9000 Ghent, Belgium

A nonlinear k–ε model is applied to predict local convective heat transfer in impinging turbulent axisymmetric jets onto a flat plate. Both the nonlinear constitutive law for the turbulent stresses and the ε transport equation improve the results. Accurate results are obtained for different geometrical setups (in particular a different nozzle-plate distance), both in terms of heat transfer and of flowfield predictions. Reynolds-number dependence of the results is discussed. Second, it is illustrated that the second-order terms in the constitutive law have a negligible influence on the results, except for the turbulent normal stress profiles. Consequently, a first-order model, with locally flow-dependent eddy viscosity, is sufficient to obtain accurate results for the complex test case under study. Comparisons are made to experimental data, to results from a low-Reynolds standard k–ε model, and to the v^2–f model.

Nomenclature

c_p	=	specific heat capacity at constant pressure
D	=	nozzle diameter
k	=	turbulent kinetic energy
Nu	=	Nusselt number
P_k	=	production of turbulent kinetic energy
Pr	=	Prandtl number
Pr_t	=	turbulent Prandtl number
p	=	pressure
$\bar{q}$	=	heat-flux vector
$\lvert q_w \rvert$	=	heat flux at flat plate, W/m^2
Re_t	=	turbulent Reynolds number
R_y	=	dimensionless distance from wall
S	=	strain rate
S_k	=	source term for k
S_ε	=	source term for ε
T	=	temperature
T_w	=	temperature at flat plate
T_0	=	temperature at nozzle exit
U_b	=	bulk velocity
$\bar{v}$	=	velocity vector
x_k	=	coordinate direction
y	=	normal distance from wall
δ_{ij}	=	Kronecker delta
ε	=	dissipation rate
η	=	nondimensional tensor invariant
κ	=	thermal conductivity
μ	=	molecular viscosity
μ_t	=	turbulent viscosity
ρ	=	density
$\bar{\bar{\tau}}$	=	stress tensor
τ_t	=	turbulent timescale
Ω	=	vorticity
∇	=	divergence/gradient

Received 24 March 2003; revision received 10 June 2003; presented as Paper 2003-3743 at the AIAA 33rd Fluid Dynamics Conference, Orlando, FL, 22–26 June 2003; accepted for publication 30 June 2003.

*Postdoctoral Fellow of the Fund of Scientific Research—Flanders (Belgium) (FWO-Vlaanderen), Department of Flow, Heat and Combustion Mechanics, Sint-Pietersnieuwstraat 41; Bart.Merci@UGent.be. Member AIAA.

†Researcher, Department of Flow, Heat and Combustion Mechanics, Sint-Pietersnieuwstraat 41.

‡Professor, Department of Flow, Heat and Combustion Mechanics, Sint-Pietersnieuwstraat 41; Erik.Dick@UGent.be. Member AIAA.

Introduction

TURBULENT convective impingement heat transfer occurs in many industrial applications (e.g., turbine blade cooling). The local Nusselt number, quantifying the local heat transfer, is an important technical quantity, for which numerical simulation results must be reliable. However, Behnia et al.[1,2] demonstrated that the stagnation-point heat transfer is dramatically overestimated by the standard k–ε model.[3]

Durbin's v^2–f turbulence model[4] provides accurate results at the cost of two additional equations: a transport equation for v^2 and an elliptic equation for f. Consequently, it is more time consuming than classical two-equation eddy-viscosity turbulence models. As pointed out by Merci and Dick,[5] a comparable quality is obtained with a nonlinear k–ε model. The discussion was focused onto an axisymmetric jet, impinging onto a flat plate, with a nozzle-plate distance equal to two jet diameters.

In this paper results are presented for a different nozzle-plate distance. Different Reynolds numbers are considered, in order to study the Reynolds dependence of experimental data and numerical results. The nonlinear k–ε model, which has also been successfully applied to a number of completely different flows,[6–8] retains its quality. This guarantees a global applicability to some extent.

In many practical turbulent flows the dominant forces result from the turbulent shear stresses. In impinging flow situations the turbulent normal stresses are also deemed important. These stresses are influenced by the second-order terms in the constitutive law. However, it is illustrated here that their effect on the flowfield, and consequently on the heat-transfer results, is small. It is illustrated in this paper that a first-order constitutive law is sufficient in order to obtain reliable results, when the eddy viscosity (in particular c_μ) depends on the local mean flowfield. The transport equation for the dissipation rate ε is also very important for the quality of the results.

Governing Equations

The steady-state transport equations are

$$\begin{cases} \nabla \cdot (\rho \bar{v}) = 0 \\ \nabla \cdot (\rho \bar{v} \bar{v}) + \nabla p = \nabla . (\bar{\bar{\tau}}) \\ \nabla \cdot (\rho T \bar{v}) = \nabla \cdot (\bar{q}/c_p) \\ \nabla \cdot (\rho k \bar{v}) = \nabla \cdot [(\mu + \mu_t/\sigma_k)(\nabla k)] + S_k \\ \nabla \cdot (\rho \varepsilon \bar{v}) = \nabla \cdot [(\mu + \mu_t/\sigma_\varepsilon)(\nabla \varepsilon)] + S_\varepsilon \end{cases} \quad (1)$$

External forces and internal heat sources are absent, and averaging symbols are omitted. Favre averages are used because the density is variable. The stress tensor contains a molecular and a turbulent part:

$$\bar{\bar{\tau}} = 2\mu S_{ij} + \bar{\bar{\tau}}^t \tag{2}$$

with S_{ij} the strain rate tensor:

$$S_{ij} = \frac{1}{2}\left(\frac{\partial v_i}{\partial x_j} + \frac{\partial v_j}{\partial x_i}\right) - \frac{1}{3}\delta_{ij}\frac{\partial v_k}{\partial x_k} \tag{3}$$

The energy equation deserves extra attention. In principle, this is an equation for total enthalpy. However, when the contributions of mean and turbulent kinetic energy are neglected and a constant c_p is assumed the equation can be rewritten in terms of mean temperature T. As was done by Behnia et al.,[1,2] the work done by the stress tensor is also neglected. Merci et al.[9] demonstrated that this is justified.

The heat flux is modeled as

$$\bar{q} = -(\mu c_p/Pr)\nabla T - (\mu_t c_p/Pr_t)\nabla T \tag{4}$$

applying the linear gradient hypothesis for the turbulent heat flux. As pointed out by Behnia et al.,[1] the use of a variable turbulent Prandtl number does not significantly improve the results. Therefore, it is kept constant: $Pr_t = 0.9$.

Model Description

A detailed development of the turbulence model is described elsewhere.[6] Only the essential parts are mentioned here. The reader is referred to the Appendix for the resulting detailed model.

Constitutive Law

The constitutive law reads

$$\tau_{ij}^t = -\rho\overline{v_i' v_j'} = -\tfrac{2}{3}\delta_{ij}\rho k + 2\mu_t S_{ij} + Q + C \tag{5}$$

The cubic term C is identically zero because there is no swirl.[6] It must be stressed here that this does not apply to the term with c_1 in expression (A1), which is considered as a first-order term. It is illustrated later that the influence of the quadratic terms Q on the results is negligible. Consequently, the constitutive law reduces to a first-order expression, with an eddy viscosity defined as

$$\mu_t = \rho f_\mu c_{\mu,\text{eff}} k\tau_t \tag{6}$$

The crucial factor in the model is $c_{\mu,\text{eff}}$ [Eq. (A10)], which depends on local tensor invariants and which includes the effect of (de)stabilizing streamline curvature on turbulence[6] (see Appendix).

Transport Equations

The transport equation for the turbulent kinetic energy k in Eqs. (1) is standard, with a source term:

$$S_k = P_k - \rho\varepsilon \tag{7}$$

$$= \tau_{ij}^t \frac{\partial v_i}{\partial x_j} - \rho\varepsilon \tag{8}$$

For ε, on the other hand, the following source term has been developed[5]:

$$S_\varepsilon = (1 - f_{R_y})c_{\varepsilon 1}(P_k/\tau_t) + f_{R_y}C_1 S\rho\varepsilon - c_{\varepsilon 2} f_2(\rho\varepsilon/\tau_t) + E + Y_c \tag{9}$$

It is a blending of the source term of Merci et al.,[10] yielding accurate values for ε in wall-dominated and rotating flows, and the one of Shih et al.,[11] suitable for high-Reynolds free shear flows. The plane jet–round jet anomaly is resolved.[6] The blending function f_{R_y} is zero near solid boundaries and unity in free shear flows.

For the test case under study in this paper, the crucial terms in Eq. (9) are the variable $c_{\varepsilon 2}$ and a length-scale correction, based on the proposal by Yap. This correction[12] improves the stagnation point heat-transfer prediction and has no effect in free shear flows. The new "production" term for the dissipation rate on itself is in principle less important for the test case in this paper, because f_{R_y} is zero in the neighborhood of the flat plate. This has already been confirmed elsewhere.[9]

Numerical Method

Equations (1) have been solved with the commercial computational-fluid-dynamics package Fluent. Second-order upwinding has been used for the convective terms in the momentum, energy, and turbulence equations. The SIMPLE algorithm is used for the pressure–velocity coupling. The segregated solver is used, implying that Eqs. (1) are solved in a sequential manner.

The numerical method differs from previous work.[5,9] A consequence is that the grid must be more refined here, as a result of higher numerical diffusion (see further: grid-refinement study).

The linearized negative parts of the source terms in the turbulence equations are treated implicitly for stability reasons. As the equations are not solved in a coupled manner, this method also differs from previous work.[13]

Test-Case Description

The test case in this paper is a round jet, impinging onto a flat plate (Fig. 1).

Experimental Setup

A fully developed turbulent airflow emerges from the nozzle exit with Reynolds number, based on jet diameter and bulk velocity U_b, $Re = \rho U_b D/\mu = 2.3 \times 10^4$ or $Re = 7 \times 10^4$. The pipe thickness is equal to $0.0313D$ (Ref. 2). At the plate a small uniform heat flux is imposed. Local temperature measurements have been performed by Baughn and Shimizu[14] Baughn et al.[15] In a later stage more experimental data sets have become available.[16,17] Despite a reported uncertainty level of about 5% by most experimentalists, there is a large spreading in the reported heat-transfer rates.

Experimental data on the flowfield have been presented by Craft et al.[18] and Cooper et al.[19]

Numerical Boundary Conditions

At the inlet boundary a (separately calculated) fully developed turbulent pipe flow is imposed in the nozzle (velocity inlet). The entrainment of air around the nozzle is described by imposing a pressure-inlet boundary condition, with atmospheric pressure and a

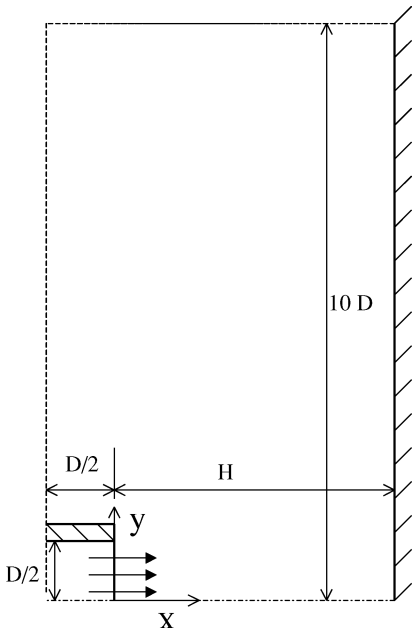

Fig. 1 Test-case geometry.

turbulence intensity of 1%. The inlet boundary of the computational domain is sufficiently far upstream of the nozzle exit (Fig. 1), so that the air entrainment is accurately reproduced. The inlet air temperature is 293 K. Static pressure is extrapolated from the flowfield.

At the plate the velocity components and turbulent kinetic energy are set to zero, and a zero derivative is used for the static pressure. The dissipation rate is determined as $\varepsilon_w = 2(\mu/\rho)[\partial\sqrt{(k)}/\partial x]^2$. A heat flux $|q_w| = 50$ W/m^2 is imposed.

At the axis symmetry boundary conditions are used. At the upper boundary atmospheric static pressure is imposed. Radial derivatives for the other quantities are set to zero (pressure-outlet condition).

Computational Grid

The basic structured computational mesh consists of 257×225 points. As already mentioned, this grid is more refined than in previous work.[5] This necessity (see further: grid-refinement study) is probably caused by a relatively larger amount of numerical diffusion.

The grid starts $1/2D$ upstream of the nozzle exit (Fig. 1). Ahead of the nozzle exit, there are 32 cells in the axial direction, with refinement near the exit so that the cells at the edge of the nozzle are square (smallest dimension, see further: $0.0313D/8 \approx D/128$). Behind the nozzle exit the nodes are distributed such that the smallest dimension is $D/128$ at the nozzle exit and $D/1000$ at the plate. The cells are stretched toward $x = H/2$.

Radially, there are 80 cells within the pipe. The mesh is refined toward the symmetry axis for accuracy reasons near the stagnation point (smallest dimension: $D/1000$). It is also refined toward the nozzle edge in order to obtain accurate coflow entrainment predictions (smallest dimension: $D/128$). The pipe thickness is equal to $0.0313D$ and contains eight equally sized cells. In the coflow the cells are stretched toward the upper boundary.

A grid-independence study is performed on the results with the present model by refinement of the grid in the two directions. This is discussed further in the paper.

Results

Results are presented for different nozzle-plate distances and Reynolds numbers. The present model consists of constitutive law (5) with $Q = C = 0$ and source term S_ε from Eq. (9). The contrast with the model, referred to as "quad," is that $Q \neq 0$ in the latter: it is obtained by means of Eqs. (A12) and (A13).

The simulation results are compared to experimental data,[14–19] to the low-Reynolds standard k–ε model by Yang and Shih[20] (YS), and to Durbin's v^2–f model.[1,2]

Stagnation Nusselt Number

The Nusselt number expresses local heat transfer and is defined as

$$Nu = \frac{D|q_w|}{\kappa(T_w - T_0)} \tag{10}$$

Table 1 gives the stagnation-point Nusselt number for $H = 2D$ and $6D$. As was already discussed elsewhere,[5] the unacceptable YS predictions are mainly, but not solely, explained by the excessive amount of turbulent kinetic energy, obtained with this model. To explain this, the Nusselt number (10) is reformulated in terms of the temperature gradient at the flat plate:

$$Nu = \frac{D|\partial(T - T_0)/\partial x|_{x=x_w}}{T_w - T_0} \tag{11}$$

Table 1 Stagnation-point Nusselt number ($Re = 2.3 \times 10^4$)

Model	$H/D = 2$	$H/D = 6$
k–ε	312	330
v^2–f[1]	150	178
Quad[5]	154	161
Present	150	156
Exp.	135–150	146–183

where the subscript w refers to the plate. This gradient is very sensitive to the flowfield because the mean temperature field is governed by a convection–diffusion equation [Eq. (1)]. As a consequence, small differences in the mean velocity profiles in the stagnation region have a large influence on the stagnation Nusselt number. It has been observed[5] that the velocity with the YS model is lower than with the present model farther from the flat plate and is higher near the plate. The behavior near the plate is governed by the axial derivative of the turbulent normal stress. Because the excessive level of turbulent kinetic energy with the YS model, the absolute level of the turbulent normal stress is much too high, and the axial derivative is also larger than with the present model. This results in a higher velocity near the flat plate, more convection of heat, and a steeper temperature gradient. This explains the large effect of excessive turbulent kinetic energy on the stagnation Nusselt number through its effect on the flowfield.[5]

Different model aspects are important for the stagnation Nusselt-number results. Firstly, the final term in definition (A6) of c_μ prevents overprediction of turbulent kinetic energy: the eddy viscosity is lowered [Eq. (6)]. Note that $|W| = 1/\sqrt{6}$ [Eq. (A7)] in the stagnation region, so that this final term is activated, while factor $(1 - f_{R_y})$ removes the term away from solid boundaries. Second, the presence of the "Yap" term (A20) in S_ε [Eq. (9)] is important, because this term also counteracts excessive production of turbulent kinetic energy. On its turn, this leads to better flowfield predictions[5] and thus to better Nusselt-number predictions. The third aspect is that the destabilizing streamline curvature effect on turbulence is desactivated in the stagnation region. This is done through the introduction of factor f_W (A9) into expression (A8). [The same factor is also introduced into the quadratic terms in Eq. (5).] Because $|W| = 1/\sqrt{6}$ in the stagnation region, this implies that f_W becomes zero. For the term in Eq. (5), multiplied by c_1, this results in a relatively lower level of turbulent kinetic energy: when $S > \Omega$, which is true at the symmetry axis, the term leads to an increase of turbulent kinetic energy.[10] By setting c_1 to zero, this is avoided.

Nusselt-Number Profile

Figure 2 shows the evolution of the Nusselt number (10) for $H = 2D$ and $6D$ along the plate. The two experimental data curves for $H = 6D$ correspond to the highest and lowest measured profiles and thus indicate the spreading of the data. For this nozzle-plate distance there is no secondary maximum in the profile, in contrast to the case $H = 2D$. The correct prediction with the present model of the secondary maximum for $H = 2D$ and the absence hereof for $H = 6D$ is caused by formulation (A6) of c_μ in the constitutive law (5). Globally, the quality of the present model is comparable to what is shown by Behnia et al.[1,2] for the v^2–f model.

Flowfield Predictions

Results are presented for $H = 6D$ and $Re = 7 \times 10^4$. The case $H = 2D$, $Re = 2.3 \times 10^4$, has already been described elsewhere.[5]

In Fig. 3 the mean velocity profiles are shown for different radial positions. At the symmetry axis ($r = 0$) differences are small, because the pressure force is the most important in the momentum x equation. Recall, however, that the small differences near the stagnation point cause the large differences in the temperature gradient and thus the stagnation point Nusselt number,[5] as just described. Away from the symmetry axis, good agreement between the present model and the experimental data is retained, in contrast to the YS model. The latter suffers from excessive diffusion: the peak velocity is too low.

Also the flow acceleration between $r = 0.5D$ and $1.5D$ is well captured with the present model. The main force in the flow is governed by the turbulent shear stress. Profiles for this stress are shown in Fig. 4. Clearly, agreement with experimental data is acceptable with the present model. All of these findings are completely in line with previous results[5] for $H = 2D$, $Re = 2.3 \times 10^4$, illustrating the present model's general applicability.

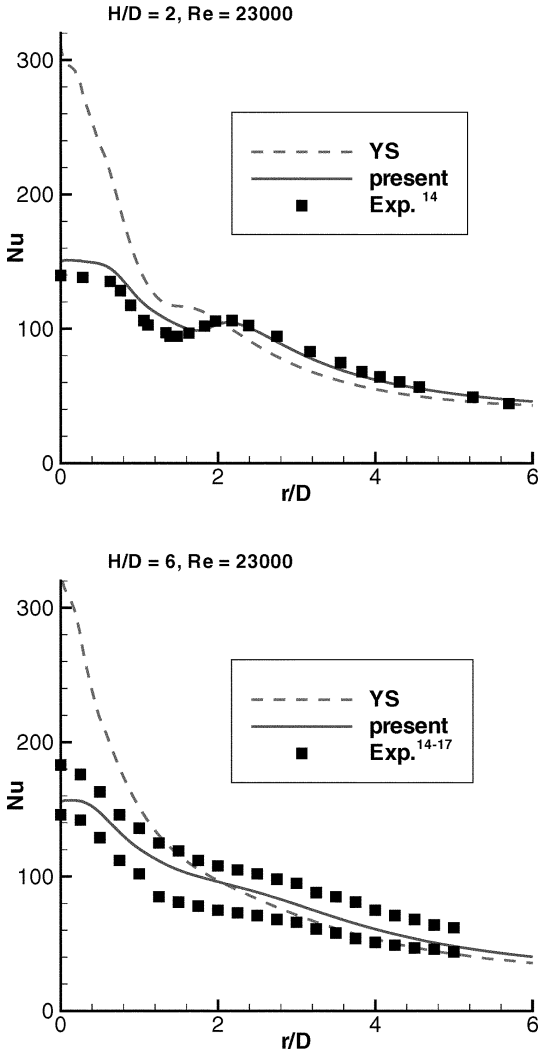

Fig. 2 Nusselt-number profiles along the plate ($Re = 2.3 \times 10^4$).

Effect of Second-Order Terms in Constitutive Law

One of the issues of this paper is that the second-order terms Q in the constitutive law (5) are not crucial. A similar conclusion has already been obtained by Apsley and Leschziner for the turbulent flow in a diffuser,[21] where the shear stresses are dominant. Here, this is confirmed for stagnating flows. As illustrated by the small differences in the profiles of the present model and the quad model in Figs. 3 and 4, the effect of the second-order terms on the flowfield is indeed small. The reason is that their main effect is on the turbulent normal stresses,[10] which have a negligible resulting force in shear-stress-driven flows (which are most common in practical situations). As already mentioned, it is illustrated here that even in stagnating flows, where normal stresses are important, their effect on the global results is small.

The preceding is confirmed in Fig. 5, showing the fields of turbulent kinetic energy obtained with the present model ($Q = 0$) and the quad model. It is known that the second-order terms have an identically zero contribution to the production term of turbulent kinetic energy, so that no direct influence on the k field should be expected. Of course, an indirect effect through a different flowfield could be possible. As just illustrated, this effect is small. Indeed, the structure (with an off-axis position of maximum turbulent kinetic energy) and the absolute values are very similar, whether $Q = 0$ or not.

Obviously, the effect of the quadratic terms is visible in the turbulent normal stress profiles (Fig. 6). As just argued, this is considered an "aesthetic," rather than a fundamental model feature. Moreover, the main influence on the turbulent normal stress profiles

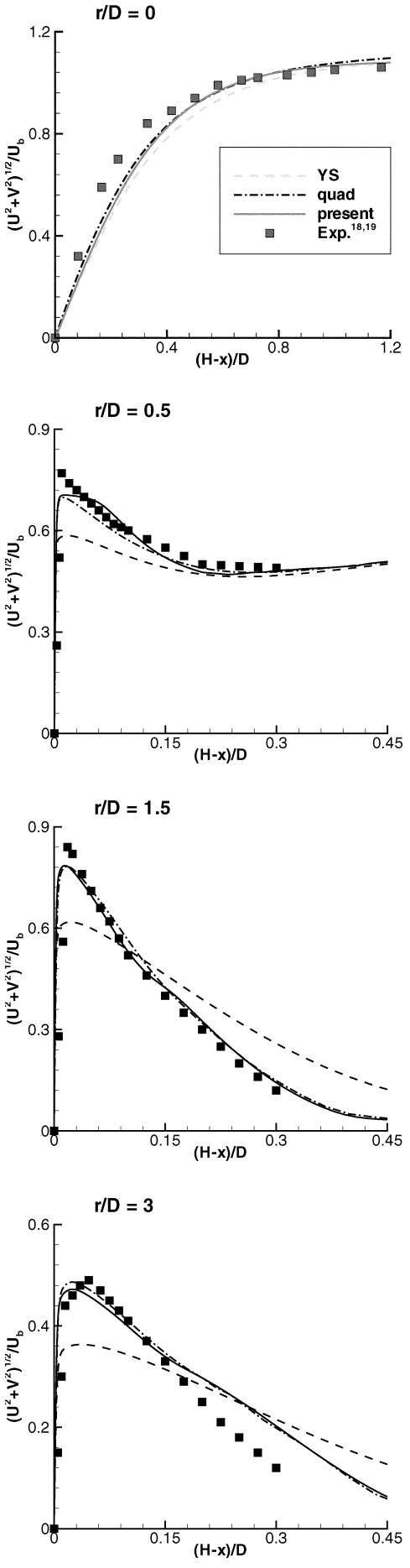

Fig. 3 Mean velocity profiles ($H/D = 6$, $Re = 7 \times 10^4$).

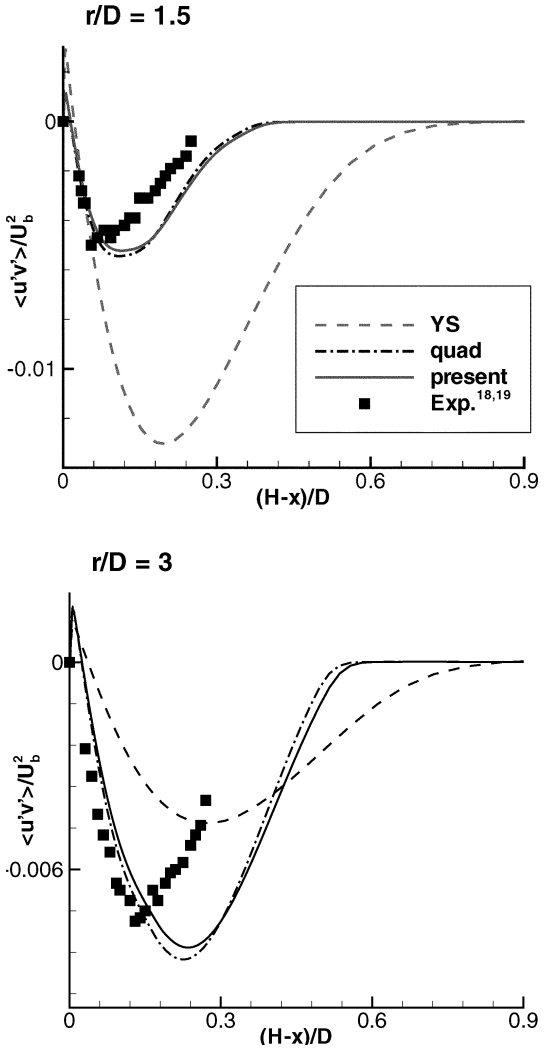

Fig. 4 Turbulent shear-stress profiles ($H/D = 6$, $Re = 7 \times 10^4$).

is the amount of turbulent kinetic energy (on which the second-order terms have only a very small influence), whereas the distribution of this energy over the different normal stresses only plays a secondary role. Consequently, the differences in the normal stress profiles are not very large. For completeness, it is mentioned that in other flows (e.g., square duct flows) normal stress anisotropy is important for secondary flow predictions, so that second-order terms are more influential. Still, it concerns only secondary flow features.

Effect of Reynolds Number on Heat Transfer

In Table 2 the stagnation Nusselt number is shown for the higher Reynolds number $Re = 7 \times 10^4$. The overprediction by the YS model, as observed in Table 1, is confirmed and even worse at the higher Reynolds number. Differences between the present model and the quad model[5] are again negligible, illustrating once more that the second-order terms in the constitutive law are not important at all. The quality of the present model in terms of the Reynolds dependence of the stagnation Nusselt number is comparable to the v^2–f model.[1]

Figure 7 confirms that also the quality of the shape of the Nusselt-number profiles is retained for $Re = 7 \times 10^4$. Again the presence or absence of a secondary maximum is correctly predicted by the present model.

Grid-Refinement Study

As already mentioned, the basic grid consists of 257×225 grid points. To test the grid independence of the results, the grid has been

Table 2 Stagnation-point Nusselt number ($Re = 7 \times 10^4$)

Model	$H/D = 2$	$H/D = 6$
k–ε	713	743
v^2–f[1]	265	300
Quad[5]	265	290
Present	264	290
Exp.	235	275

Table 3 Coordinates of monitoring points

Point	x/D	r/D
A	5.8	0
B	5.8	1

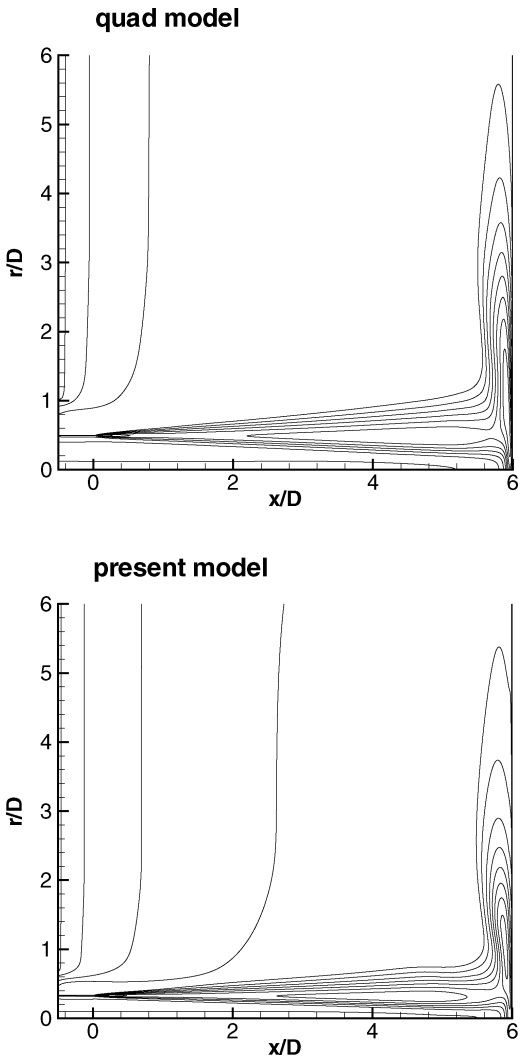

Fig. 5 Fields of turbulent kinetic energy ($H/D = 6$, $Re = 2.3 \times 10^4$).

refined and coarsened in both directions. The velocity components, turbulent kinetic energy, and dissipation rate have been monitored in two points. The coordinates of the monitoring points are given in Table 3. Point A is on the symmetry axis in the stagnation region, whereas point B is near the position of maximum turbulent kinetic energy (Fig. 5).

The results of the grid-refinement study are summarized in Tables 4 and 5. Clearly, the differences between the values of the different monitored values in both points are small for the basic grid and the refined grid (513×449 points). Huge differences exist, however,

Table 4 Grid-refinement study for two monitoring points ($H/D = 6$, $Re = 7 \times 10^4$)

Point	Quantity	129×113	257×225	513×449
A	U/U_b	1.66	1.66	1.66
A	V/U_b	0	0	0
A	k/U_b^2	4.24×10^{-3}	1.18×10^{-2}	1.17×10^{-2}
A	$\varepsilon D/U_b^3$	5.53×10^{-4}	2.67×10^{-3}	2.69×10^{-3}
B	U/U_b	3.96×10^{-1}	3.46×10^{-1}	3.42×10^{-1}
B	V/U_b	1.16	1.25	1.24
B	k/U_b^2	1.13×10^{-2}	1.99×10^{-2}	1.96×10^{-2}
B	$\varepsilon D/U_b^3$	5.40×10^{-3}	1.94×10^{-1}	1.92×10^{-1}

Table 5 Grid-refinement study for stagnation-point Nusselt number ($H/D = 6$, $Re = 7 \times 10^4$)

Grid	Nu_{stag}
129×113	250
257×225	290
513×449	289

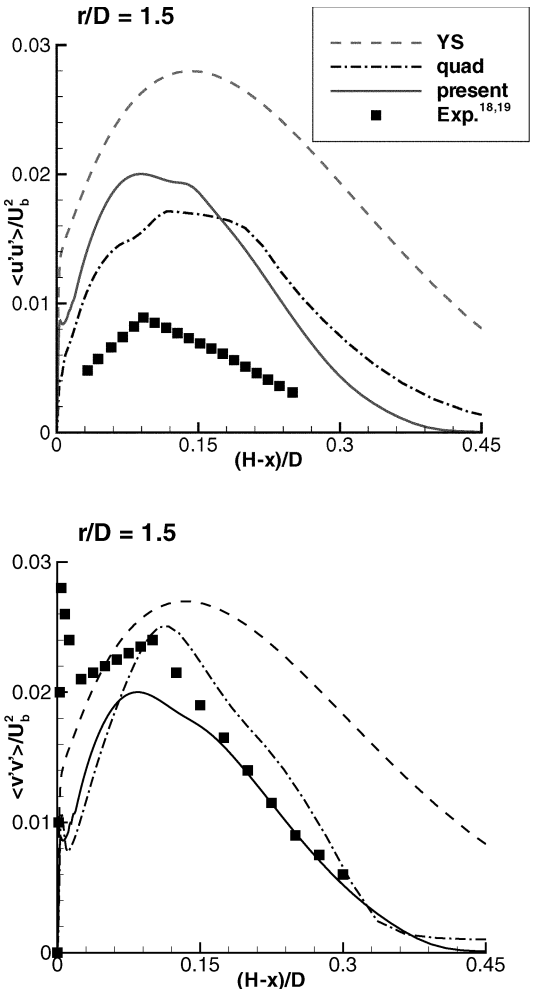

Fig. 6 Turbulent normal stresses, parallel and perpendicular to the plate ($H/D = 6$, $Re = 7 \times 10^4$).

between the results on the coarsened grid (129×113 points). The obvious conclusion is that the latter is too coarse. This is in contrast with previous work[5,9] because of the differences in the numerical method, as already mentioned.

This is confirmed in the results for the stagnation Nusselt number, given in Table 5: the value is practically identical on the basic and the refined grid, whereas it is substantially different from what is obtained on the coarser grid.

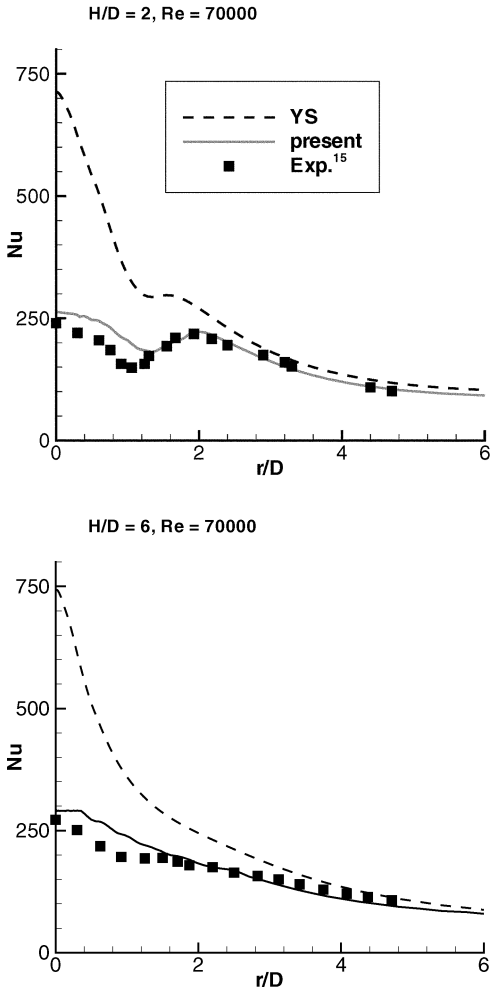

Fig. 7 Nusselt-number profiles along the plate ($Re = 7 \times 10^4$).

Conclusions

Results have been presented with a k–ε model for the local convective heat transfer in round turbulent jets, impinging onto a flat plate.

Because a global discussion for a nozzle-plate distance H equal to two jet diameters and Reynolds number $Re = 2.3 \times 10^4$ has already been given elsewhere,[5] attention in this paper was focused onto the case $H = 6D$. It was illustrated that the Nusselt-number profile along the plate is very well predicted, for both $Re = 2.3 \times 10^4$ and $Re = 7 \times 10^4$. This is mainly because of the locally flow-dependent definition of the eddy viscosity [through $c_{\mu,\text{eff}}$, Eq. (A10)] and because of the ε transport equation.

It was illustrated that good agreement is obtained between the present model's mean velocity profiles and experimental data at different radial positions. Again, both the constitutive law and the ε equation contribute to this success.

The second-order terms in the constitutive law of the already developed k–ε model[5] have a negligible effect on the main results, despite the stagnation region. The reason is that the resulting force of the turbulent normal stresses is small in comparison to the turbulent shear stress force or in comparison to the pressure force. The important consequence hereof is that the constitutive law can be restricted to a first-order relationship, as long as the eddy viscosity is defined such that streamline curvature and/or rotation effects are incorporated.

The effect of the Reynolds number on the results has been investigated. The present model retains its quality at the higher Reynolds number, indicating its general applicability.

Finally, a grid-refinement study has been performed. It was illustrated that the obtained results are indeed grid independent. A

more refined grid was found to be necessary, compared to previous work,[5,9] because of the differences in the numerical methods.

The results of this paper, in combination with previous results,[5] indicate the general validity of the present model.

Appendix: Turbulence Model

The turbulent stresses are modeled as

$$\begin{aligned}\tau_{ij}^t = -\rho\overline{v_i' v_j'} = &-\tfrac{2}{3}\delta_{ij}\rho k + 2\rho f_\mu c_\mu k\tau_t S_{ij}\\ &- c_1\rho k\tau_t^3(S_{mn}S_{nm} + \Omega_{mn}\Omega_{nm})S_{ij}\\ &- q_1\rho k\tau_t^2\left(S_{ik}S_{kj} - \tfrac{1}{3}\delta_{ij}S_{lm}S_{ml}\right)\\ &- (q_2 + q_1/6)\rho k\tau_t^2(\Omega_{ik}S_{kj} - S_{ik}\Omega_{kj})\\ &- c_2\rho k\tau_t^3(\Omega_{ik}S_{kl}S_{lj} - S_{ik}S_{kl}\Omega_{lj})\end{aligned} \tag{A1}$$

with S_{ij} from Eq. (3) and the vorticity tensor components defined as

$$\Omega_{ij} = \frac{1}{2}\left(\frac{\partial v_i}{\partial x_j} - \frac{\partial v_j}{\partial x_i}\right) \tag{A2}$$

The turbulent timescale is given by

$$\tau_t = \frac{k}{\varepsilon} + \sqrt{\frac{\mu}{\rho\varepsilon}} \tag{A3}$$

The coefficients in Eq. (A1) depend on the invariants:

$$S = \sqrt{2S_{ij}S_{ij}}, \qquad \Omega = \sqrt{2\Omega_{ij}\Omega_{ij}} \tag{A4}$$

$$\eta = \tau_t(S^2 + \Omega^2)^{\frac{1}{2}} \tag{A5}$$

The expression for c_μ is

$$c_\mu = \left[A_1 + A_s\eta + 25\left(1 - f_{R_y}\right)|W|\right]^{-1} \tag{A6}$$

with $R_y = \rho\sqrt{(k)}y/\mu$, $A_1 = 4$, $A_s = \sqrt{(3)}\cos\phi$ and $\phi = \frac{1}{3}\arccos(\sqrt{(6)}W)$, where W is defined as

$$W = 2^{1.5}\frac{S_{ij}S_{jk}S_{ki}}{S^3} \tag{A7}$$

The final term in Eq. (A6) prevents overprediction of turbulent kinetic energy in stagnation regions.

The coefficient c_1 is defined as

$$\begin{cases} S \geq \Omega : c_1 = -f_W \min\left(40c_\mu^4; 0.15\right)\\ S < \Omega : c_1 = -f_W \min\Big[\min\left(600c_\mu^4; 0.15\right);\\ \qquad 4f_\mu c_\mu\Big/\left(\Omega^2\tau_t^2 - S^2\tau_t^2\right)\Big]\end{cases} \tag{A8}$$

where f_W is defined as

$$f_W = 1 - 18|W|^2 + \left(72\Big/\sqrt{6}\right)|W|^3 \tag{A9}$$

The introduction of f_W improves heat-transfer results in stagnation regions because it also avoids excessive turbulent kinetic energy production because of destabilizing streamline curvature.[5]

The two first-order terms in expression (A1) can be combined. The eddy viscosity can then be defined with an effective $c_{\mu,\text{eff}}$ [Eq. (6)]:

$$c_{\mu,\text{eff}} = c_\mu - \tfrac{1}{4}(c_1/f_\mu)\tau_t^2(S^2 - \Omega^2) \tag{A10}$$

The damping function f_μ is

$$f_\mu = 1 - \exp\left(-6\,10^{-2}\sqrt{R_y} - 2\,10^{-4}R_y^{1.5} - 2\,10^{-8}R_y^4\right) \tag{A11}$$

The coefficients q_1 and q_2 are

$$q_1 = (7 + 2.1\eta + 0.0042\eta^3)^{-1} \tag{A12}$$

$$q_2 = (10 + 3.6\eta + 0.01\eta^3)^{-1} \tag{A13}$$

The coefficient c_2 is equal to $c_2 = -2c_1$.

The transport equation for the turbulent kinetic energy k is standard. For ε a combined transport equation is used[5]:

$$\begin{aligned}\frac{\partial}{\partial x_j}(\rho\varepsilon v_j) = &\left(1 - f_{R_y}\right)c_{\varepsilon 1}\frac{P_k}{\tau_t} + f_{R_y}C_1 S\rho\varepsilon\\ &- c_{\varepsilon 2}f_2\frac{\rho\varepsilon}{\tau_t} + \frac{\partial}{\partial x_j}\left[\left(\mu + \frac{\mu_t}{\sigma_\varepsilon}\right)\frac{\partial\varepsilon}{\partial x_j}\right] + E + Y_c\end{aligned} \tag{A14}$$

The blending function f_{R_y} is defined as

$$f_{R_y} = \tfrac{1}{2} + \tfrac{1}{2}\sin[(\pi/2)\min(F; 1)] \tag{A15}$$

$$F = \max(R_y/500 - 3; -1) \tag{A16}$$

with R_y as just defined. The function goes from 0 to 1 in the interval $R_y = 1000$ to $R_y = 2000$.

The model constant $c_{\varepsilon 1} = 1.44$ is standard. The strain rate S is obtained from Eq. (A4), and the parameter C_1 is

$$C_1 = \max\left(0.43; \frac{S\tau_t}{5 + S\tau_t}\right) \tag{A17}$$

The parameter $c_{\varepsilon 2}$ is

$$c_{\varepsilon 2} = \max\left(1.83 + \frac{0.075\tau_t\Omega}{1 + \tau_t^2 S^2}; C_2 f_{R_y}\right) \tag{A18}$$

with $C_2 = 1.9$. The damping function f_2 is $f_2 = 1 - 0.22\exp(-Re_t^2/36)$, with $Re_t = \rho k\tau_t/\mu$ the turbulent Reynolds number and the model constant σ_ε is $\sigma_\varepsilon = 1.2$. The low-Reynolds source term E has been obtained from the k–ω model[10]

$$E = -1.8(1 - f_\mu)\left(\mu + \frac{\mu_t}{\sigma_\varepsilon}\right)\frac{\partial k}{\partial x_i}\frac{\partial\tau_t^{-1}}{\partial x_i} \tag{A19}$$

with f_μ from Eq. (A11).

The Yap correction[12] is implemented as

$$\begin{cases} S \leq 1.05\Omega : Y_c = 0\\ S > 1.05\Omega : Y_c = 0.13\left(1 - f_{R_y}\right)(k^2/y^2)\\ \qquad \times \max\left[\left(0.4k^{\frac{3}{2}}\Big/\varepsilon y - 1\right); 0\right]\end{cases} \tag{A20}$$

It is only added when streamline curvature has a destabilizing effect on turbulence ($S > \Omega$), with a factor 1.05 in order to avoid numerical problems in regions where $S \approx \Omega$.

References

[1]Behnia, M., Parneix, S., and Durbin, P. A., "Prediction of Heat Transfer in an Axisymmetric Turbulent Jet Impinging on a Flat Plate," *International Journal of Heat and Mass Transfer*, Vol. 41, No. 12, 1998, pp. 1845–1855.

[2]Behnia, M., Parneix, S., Shabany, Y., and Durbin, P. A., "Numerical Study of Turbulent Heat Transfer in Confined and Unconfined Impinging Jets," *International Journal of Heat and Fluid Flow*, Vol. 20, No. 1, 1999, pp. 1–9.

[3]Jones, W. P., and Launder, B. E., "The Prediction of Laminarization with a Two-Equation Model of Turbulence," *Journal of Heat and Mass Transfer*, Vol. 15, No. 2, 1972, pp. 301–314.

[4]Durbin, P., "Near-Wall Turbulence Closure Without Damping Functions," *Theoretical and Computational Fluid Dynamics*, Vol. 3, No. 1, 1991, pp. 1–13.

[5]Merci, B., and Dick, E., "Heat Transfer Predictions with a Cubic k–ε Model for Axisymmetric Turbulent Jets Impinging onto a Flat Plate," *International Journal of Heat and Mass Transfer*, Vol. 46, No. 3, 2003, pp. 469–480.

[6]Merci, B., and Dick, E., "Predictive Capabilities of an Improved Cubic k–ε Model for Inert Steady Flows," *Flow, Turbulence and Combustion*, Vol. 68, No. 4, 2002, pp. 335–358.

[7]Merci, B., Dick, E., Vierendeels, J., Roekaerts, D., and Peeters, T. W. J., "Application of a New Cubic Turbulence Model to Piloted and Bluff-Body Diffusion Flames," *Combustion and Flame*, Vol. 126, Nos. 1–2, 2001, pp. 1533–1556.

[8]Merci, B., Dick, E., and De Langhe, C., "Application of an Improved ε-Equation to a Piloted Jet Diffusion Flame," *Combustion and Flame*, Vol. 131, No. 4, 2002, pp. 465–468.

[9]Merci, B., Vierendeels, J., De Langhe, C., and Dick, E., "Numerical Simulation of Heat Transfer of Turbulent Impinging Jets with Two-Equation Turbulence Models," *International Journal of Numerical Methods for Heat and Fluid Flow*, Vol. 13, No. 1, 2003, pp. 110–132.

[10]Merci, B., De Langhe, C., Vierendeels, J., and Dick, E., "A Quasi-Realizable Cubic Low-Reynolds Eddy-Viscosity Turbulence Model with a New Dissipation Rate Equation," *Flow, Turbulence and Combustion*, Vol. 66, No. 2, 2001, pp. 133–157.

[11]Shih, T. H., Liou, W. W., Shabbir, A., Yang, Z., and Zhu, J., "A New k–ε Eddy Viscosity Model for High Reynolds Number Turbulent Flows," *Computers and Fluids*, Vol. 24, No. 3, 1995, pp. 227–238.

[12]Craft, T. J., Iacovides, H., and Yoon, J. H., "Progress in the Use of Non-Linear Two-Equation Models in the Computation of Convective Heat-Transfer in Impinging and Separated Flows," *Flow, Turbulence and Combustion*, Vol. 63, Nos. 1–4, 2000, pp. 59–80.

[13]Merci, B., Steelant, J., Vierendeels, J., Riemslagh, K., and Dick, E., "Computational Treatment of Source Terms in Two-Equation Turbulence Models," *AIAA Journal*, Vol. 38, No. 11, 2000, pp. 2085–2093.

[14]Baughn, J. W., and Shimizu, S., "Heat Transfer Measurements from a Surface with Uniform Heat Flux and an Impinging Jet," *Journal of Heat Transfer*, Vol. 111, Nov. 1989, pp. 1096–1098.

[15]Baughn, J. W., Hechanova, A., and Yan, X., "An Experimental Study of Entrainment Effects on the Heat Transfer from a Flat Surface to a Heated Circular Impinging Jet," *Journal of Heat Transfer*, Vol. 113, No. 4, 1991, pp. 1023–1025.

[16]Yan, X., "A Preheated-Wall Transient Method Using Liquid Crystals for the Measurement of Heat Transfer on External Surfaces and in Ducts," Ph.D. Dissertation, Dept. of Mechanical and Aeronautical Engineering, Univ. of California, Davis, CA, 1993.

[17]Lytle, D., and Webb, B., "Air Jet Impingement Heat Transfer at Low Nozzle-Plate Spaces," *International Journal of Heat and Mass Transfer*, Vol. 37, No. 12, 1994, pp. 1687–1697.

[18]Craft, T. J., Graham, L. J. W., and Launder, B. E., "Impinging Jet Studies for Turbulence Model Assessment—II. An Examination of the Performance of Four Turbulence Models," *International Journal of Heat and Mass Transfer*, Vol. 36, No. 10, 1993, pp. 2685–2697.

[19]Cooper, D., Jackson, D. C., Launder, B. E., and Liao, G. X., "Impinging Jet Studies for Turbulence Model Assessment—I. Flow Field Experiments," *International Journal of Heat and Mass Transfer*, Vol. 36, No. 10, 1993, pp. 2675–2684.

[20]Yang, Z. Y., and Shih, T. H., "A New Time Scale Based k–ϵ Model for Near-Wall Turbulence," *AIAA Journal*, Vol. 31, No. 7, 1993, pp. 1191–1198.

[21]Apsley, D. D., and Leschziner, M. A., "Advanced Turbulence Modelling of Separated Flow in a Diffuser," *Flow, Turbulence and Combustion*, Vol. 63, No. 1–4, 2000, pp. 81–112.